Journal of Alloys and Compounds 509 (2011) 4284–4289

Contents lists available at ScienceDirect

Journal of Alloys and Compounds

journal homepage: www.elsevier.com/locate/jallcom

Initial microstructural study of a Ce–La alloy using electron backscattered diffraction

Thomas B. Scott[a,*], Charles M. Younes[a], Michael Ling[b], Christopher P. Jones[a], John A. Nicholson[a], Peter J. Heard[a], Roderick Jenkins[b]

[a] Interface Analysis Centre, University of Bristol, 121 St Michael's Hill, Bristol BS2 8BS, UK
[b] AWE, Aldermaston, Reading, Berkshire RG7 4PR, UK

ARTICLE INFO

Article history:
Received 22 September 2010
Received in revised form
29 December 2010
Accepted 3 January 2011
Available online 4 January 2011

Keywords:
Metals and alloys
Microstructure
Oxidation
Surface electron diffraction

ABSTRACT

To better understand and exploit the unique electronic and structural properties of f-block metals and their alloys it is perceived that an improved knowledge of the microstructural characteristics and phase changes as a function of temperature and pressure, is necessary. For other different types of metallic systems, the use of electron back-scattered diffraction (EBSD) is becoming a common practice in order to obtain detailed microstructural information, but this has, as yet, been very limited in case of f-block metals. Because of their extreme affinity to oxygen and rapid surface reaction, EBSD studies of this metal-category are very sparse with only one work published on cerium metal providing an example of technical hurdles for a prerequisite oxide-free metal surface. Specifically the need to remove the oxide by ion etching was considered essential to enable a successful EBSD analysis. The current work presents the results of a first attempt to characterise the microstructure of a Ce–La alloy using EBSD. It demonstrates that high quality diffraction patterns and crystal orientation maps can be successfully obtained following a carefully controlled preparation of the alloy surface in the open laboratory by applying a simple and reproducible electro-polishing procedure without a further need for ion etching in vaccuo.

1. Introduction

Lanthanide metals are characteristically dense possessing high melting points and good heat conductivity. They alloy relatively easily with other metals, especially iron (e.g. misch-metal and pyrophoric alloys), and found various applications in the industry such as the production of ignition devices, e.g. tracer bullets, electron sources and superconductors. Due to their unique electronic and magnetic properties they also found applications in storage devices with some of their oxypnictides being developed for large scale production of high-temperature superconductor-PCBs and wires [1,2]. In addition, there is a very active research, amongst many others in the field of supramolecular chemistry, on the use of lanthanide f-ions for the development of luminescent complexed supramolecular structures and self-assemblies that exploit the physical and optical properties of the lanthanides for applications in luminescent switches, sensors, energy-saving lighting devices, displays, lasers, optical fibres and amplifiers as well as responsive luminescent stains for biomedical analyses and in cellulo-sensing and imaging. This particular research field has been the scope of many recent reviews such those in [3–5], to name just a few. Additionally, lanthanide based bulk metallic glasses have attracted increasing interest due to their unique properties and potential applications as functional glassy materials. These materials display many fascinating properties such as heavy fermion behaviour, thermoplastic properties near room temperature, excellent magnetocaloric effect, hard magnetism, and polyamorphism, all of which are of interest not only for basic research but also for metallurgy and technology [6–7].

The lanthanide series comprises the elements 58 (Ce) to 71 (Lu), with La (57) as a prototype of this series. It is widely accepted that lanthanides share a common outer electronic configuration; differing only in the number of 4f electrons [8]. These chemically inert 4f electrons set up localized magnetic moments, which are coupled via an indirect exchange interaction involving the conduction electrons. This leads to the formation of a wide range of magnetic structures, the periodicity of which is often incommensurate with the underlying crystal lattice [9]. For example, recent work examining gadolinium has demonstrated that the magnetic structures of the heavy rare-earth elements are unequivocally linked to their lattice parameters [10] with a trend from ferromagnetism to incommensurate ordering occurring as the atomic number or nuclear charge increases, connected to the concomitant decrease in unit cell often termed as the lanthanide contraction [11].

* Corresponding author. Tel.: +44 117 3311176.
E-mail address: t.b.scott@bristol.ac.uk (T.B. Scott).

0925-8388/$ – see front matter.
doi:10.1016/j.jallcom.2011.01.002

In order to better exploit the above mentioned properties of the 4f-block metals, it is perceived that an improved understanding of the crystal structure at low and high temperatures as well as the concomitant phase change and oxidation behaviour is necessary. Since most of these properties are greatly influenced by the surface state and bulk structure of the material, a detailed characterisation would be highly desirable. While a structural characterisation at the macro-scale can be made using conventional metallographic methods, characterisation at a micro and a nano scale is typically performed by employing a variety of complementary techniques, such as transmission electron microscopy, scanning probe microscopy and EBSD. However, one of the major obstacles for using the latter, which provides information at a much wider scale than the former techniques, is that all f-block metals are highly electropositive and consequently tarnish rapidly upon exposure to air, due to their high reactivity with oxygen [12]. In the case of cerium, such a rapid reaction leads to the formation of a surface oxide layer approximately 10 nm thick in only a few minutes as it is the most reactive of all lanthanide elements. Consequently, after surface preparation, it is very difficult to maintain an oxide free metal surface suitable for EBSD analysis. This difficulty stems from the fact that at a thickness greater than 3–4 nm the surface oxide layer will block the escape of coherently backscattered electrons, thus hindering detection and acquisition of a high quality diffraction pattern [13].

For this reason, reports on successful EBSD surveys of the 4f-block metals are rare, with the exception of one work performed by Boehlert et al. [14] on a cerium metal. These authors performed ion sputtering in an Auger system to remove the oxide layer from the sample surface after mechanical polishing. The sample was then placed in a vacuum suitcase and transferred to a scanning electron microscope equipped with an EBSD system. Also in reference to this procedure EBSD data was provided but no orientation maps were obtained. The preparatory procedure adopted is obviously time-consuming and requires specialist and expensive equipment to clean the metal surface and overcome re-oxidation during sample transfer from the ion sputtering chamber to the SEM/EBSD instrument. Furthermore, ion sputtering is known to induce surface roughness due to uneven cleaning of the surface. This roughness is generated by preferential etching of the surface which is linked to the orientation of metal grains intersecting the ion-etched surface. The alteration of the surface leads to a loss in the quality and intensity of the observed diffraction pattern [13]. Ion bombardment is also bound to produce an implantation of the incident ion-species into the metal, the extent of which is dependent on the time-duration of the ion etching sequence and the ion flux applied. The effect of ion implantation in cerium, though still unknown, could induce a modification of the metal crystal lattice in the surface and sub-surface areas which, in turn, lead to an erroneous interpretation and analysis of the EBSD data.

The current investigation has sought to develop a more appropriate and accessible method of sample preparation such that EBSD surveys of the lanthanide metals and their alloys is readily achievable. A Ce–La alloy was selected as a candidate material for this purpose, with Ce generally considered to be the more chemically reactive of the 4f-block metals family [15]. Concurrently the current work was aimed at providing the first successfully recorded EBSD data from the surface of this type of alloys, in addition to gaining an insight on the microstructure of the alloy studied as well as its phase structure at room temperature.

2. Experimental

2.1. Material and sample preparation

The alloy used in this study was made from ingots of 99.9% pure Cerium and Lanthanum purchased from Goodfellow™. The ingots were cut down to remove surface oxides and small clean pieces of both metals were weighed out to obtain a ratio of 95 wt% Ce to 5 wt% La. The metal pieces were then placed on a water-coolable copper hearth inside an arc furnace. Prior to melting the metal pieces, the furnace chamber was pumped down and purged with Ar three times with Ti metal, acting as a getter, added to purify the Ar gas stream. The Ce and La pieces were then repeatedly melted under argon at temperatures marginally in excess of 918 °C (the melting temperature of La) to get a well mixed homogenous alloy. The resulting alloy ingot was subsequently cooled under the Ar gas stream and then sealed in a quartz tube, backfilled with Ar, to protect the surface from oxidation.

In preparation for micro-structural analysis, a number of specimens, ovals approximately 8 mm × 15 mm in diameter and 1.2 mm thick, were cut from the alloy sample, perpendicular to the long-axis of the ingot, using a low-speed rotary diamond saw with rapeseed oil as lubricant. The latter was chosen because of its moderate viscosity, non-volatility and non-toxicity. This method of cutting was selected as the only practicable means of keeping atmospheric oxygen and water away from the cut metal surfaces. Sequential grinding of the specimens was performed on SiC papers up to P4000 grade with rapeseed oil as a lubricant. Between grades IPA (isopropyl alcohol—C_3H_8O) and an ultrasonic bath were used to remove grinding debris. IPA was chosen because it proved to possess the right combination of miscibility, wettability and surface tension properties to spontaneously displace the oil from the specimens. Further specimens were prepared in a similar way but by cutting parallel to the long-axis of the ingot.

Following grinding, the specimens were electro-polished for 30–60 s in an electrolyte consisting of absolute methanol (CH_3OH) and 5% perchloric acid ($HClO_4$) maintained at a constant temperature of −60 °C throughout the polishing operation using dry ice. The current density applied was approximately 1.8 A/cm^2. After washing in methanol to remove acid residues, the specimen was rapidly transferred into a SEM fitted with an EBSD system.

2.2. Sample analysis methods

Analysis with EBSD was performed in a Zeiss EVO MA10 SEM fitted with LaB_6 electron source and a Digiview 3 high speed camera with associated EBSD instrumentation from EDAX. Data was recorded and processed using OIM™ software. Orientation maps were obtained for predefined surface areas up to approximately 1 mm^2 using an automated mapping routine that recorded and indexed the diffraction patterns at regular spatial intervals, typically 2 μm for large areas and 50 nm for small area, high spatial resolution maps.

The microstructure of the alloy was further examined in a focused ion beam (FIB) instrument (FEI FIB-201 model) operated under a background pressure of less than 10^{-5} mbar. The ion beam was used first to remove the surface oxide from defined areas and expose the underlying metal for examination. Micro-sectioning to a depth of 10 μm was additionally performed to produce finely polished cross-sectional faces such that the microstructure could be examined deeper into the specimen. In such cases a protective layer of platinum, 1 μm thick, was deposited prior to sectioning in order to protect the surface of the section from ion implantation damage.

A SIMS system, equipped with a focused gallium ion source and a double-focusing magnetic sector mass analyser was also employed to provide information on the chemical homogeneity and metal purity. The analysis was performed in a positive ion mode with ion maps of the alloy surface recorded. In preliminary analyses, Ce^+ and La^+ ion clusters (peaks at mass 140 and 139 respectively) were observed to be representative of the metal, while masses 176 and 155 were considered to be associated with the oxide ion clusters CeO_2^+ and LaO^+.

Supplementary analysis was performed using X-ray diffraction (XRD) to determine the phases present within the bulk of the sample. Measurements were made using a Phillips X-Pert Pro diffractometer, with Cu-Kα radiation. To prevent significant sample oxidation during analysis the sample was pre-coated with a thin protective layer of gold (<100 nm thickness) using a sputter coater. Additionally a narrow range (20–60°) was adopted for data acquisition such that measurements took no more than 50 min to complete.

3. Results and discussion

Preliminary analysis of suitably prepared alloy surfaces using X-ray diffraction (XRD) identified the material crystal structure as fcc with diffraction peaks that could be indexed to the (1 1 1), (2 0 0), (2 2 0) and (3 1 1) reflections of the γ-phase of metallic cerium, with a lattice constant of 5.180 Å. This compares to a value of 5.150 Å for pure cerium and represents a 0.6% increase in lattice parameter considered to arise from incorporation of lanthanum into the crystal structure. Additionally the XRD analysis indicated the presence of a minor amount of oxide (as CeO_2), as shown in Fig. 1.

Subsequent examination of mechanically polished and electro-polished surfaces of the alloy revealed a marked difference in surface morphology, as can be seen in Fig. 2. Examination of

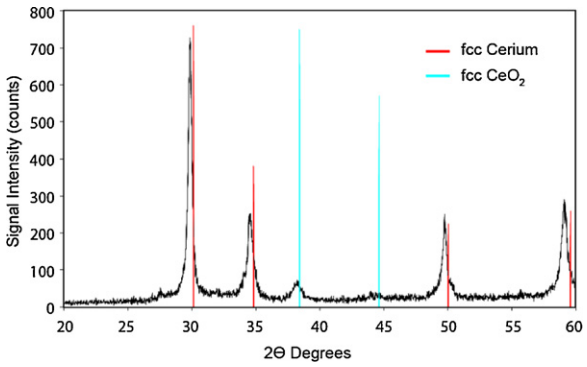

Fig. 1. X-ray diffraction pattern of a polished face of the Ce–La alloy studied.

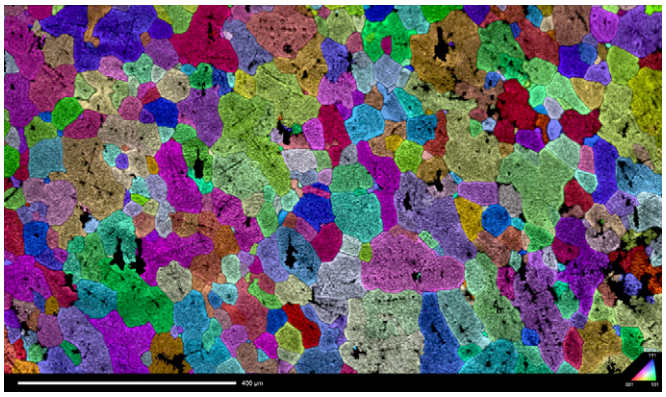

Fig. 3. EBSD orientation map of the alloy surface cut perpendicularly to the starting ingot longitudinal axis.

both samples under SEM confirmed the efficacy and reproducibility of the electro-polishing procedure developed for this study in removing most of the oxide that remained following grinding on the SiC papers. The electro-polished surface was relatively flat, with regions of the exposed metal proximal to grain boundaries slightly raised relative to the grain interiors, which were finely pitted. The average grain-size of the alloy determined from the recorded secondary electron images was approximately 80 μm, with these images also highlighting the presence of numerous particles, ascribed to oxide, present on the alloy surface.

EBSD data was successfully recorded from large areas comprising over 3000 grains, indicating that the electro-polishing time applied was sufficient to produce a clean metal surface, that was passivated long enough to allow for transfer to the SEM system without significant regrowth of the oxide, i.e. <2–3 nm thickness. The recorded EBSPs were of high quality such that high speed mapping could be performed. In all cases these patterns exhibited a good match to a cerium fcc γ-phase from the OIM materials database.

Figs. 3 and 4 illustrate inverse pole figure grain orientation maps taken from the alloy specimens cut perpendicular to each other. The maps clearly show that most of the grains in both longitudinal and transverse directions were equi-axed, exhibiting an average grain diameter of 82 μm and average grain area of 1000 μm^2. Approximately 70% of the grains were between 50 and 110 μm in diameter, with all grains displaying relatively straight grain-boundary contacts and no evidence for crystal twinning. Analysis of misorientation angle between grains indicates that the majority of grain boundaries can be classified as high angle (>30°), although a significant proportions of low-angle boundaries and sub-boundaries were indicated by the data (Fig. 5).

This was most obvious in some of the large grains observed, where multiple low angle sub-boundaries and other gradational orientation changes could be determined using crystal orientation variation plots (Fig. 6).

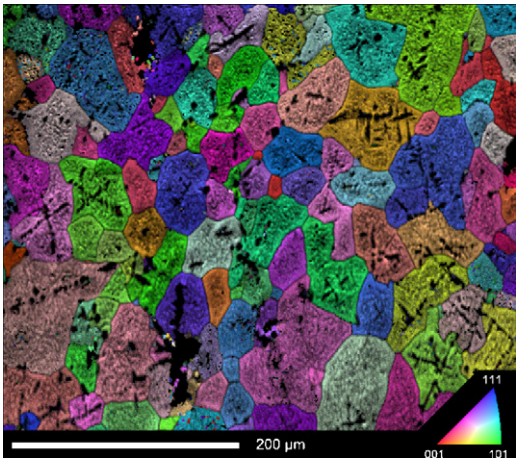

Fig. 4. EBSD orientation map of the alloy polished face cut parallel with the long axis of the starting ingot.

No clearly preferred grain orientation or orientation relationship was exhibited on the basis of the pole figure and texture plot analysis (Fig. 7). This microstructure, which formed during cooling from a molten state after repeated melting, was expected on the basis of phase equilibria considerations [16–18].

The fine surface pitting observed by secondary electron microscopy (SEM) was clearly evidenced by the recorded EBSD maps. For certain points on the alloy surface, topographic shadowing was observed to block the escape of some backscattered electrons to the EBSD detector causing the recorded diffraction patterns to be only partially complete, and therefore less reliably indexed by the software. The more etch-resistant inter-granular rims returned better quality EBSD data.

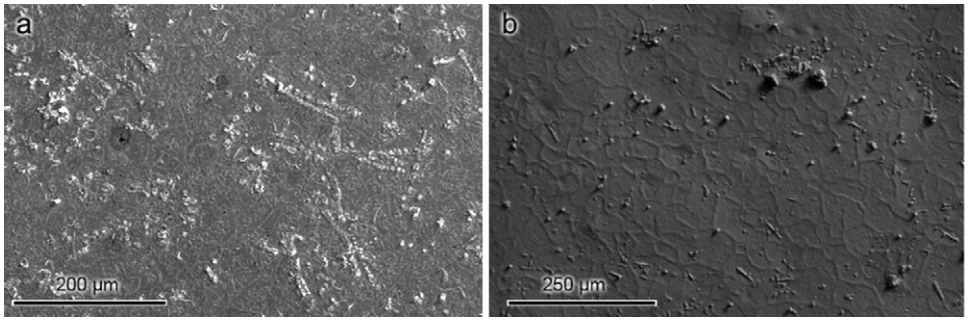

Fig. 2. Secondary electron images of the alloy after (a) grinding and mechanical polishing and (b) electro-polishing.

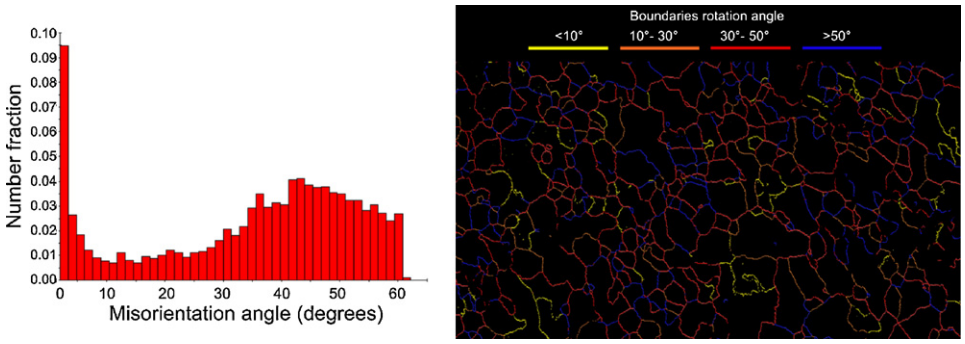

Fig. 5. A grain boundary misorientation plot (left) and grain boundary rotation angle map (right) highlighting the predominance of high-angle grain boundaries in the alloy microstructure.

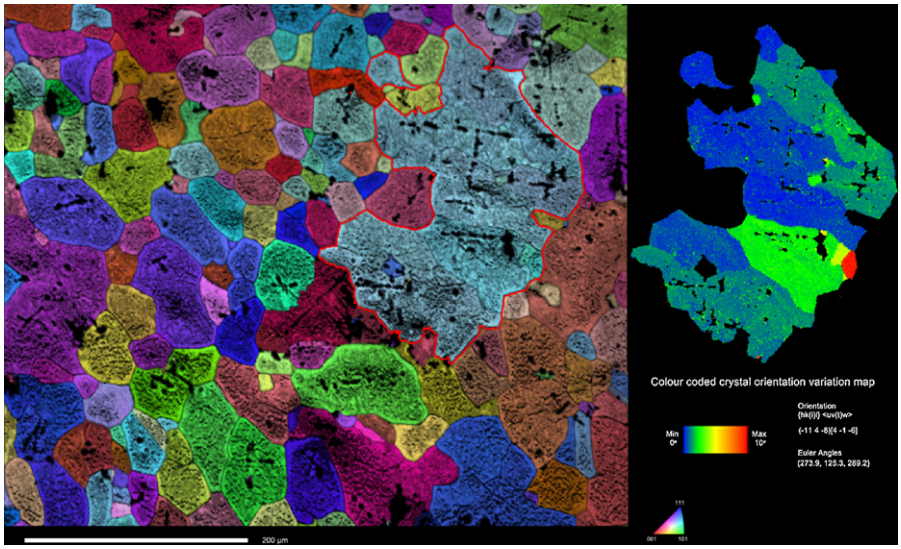

Fig. 6. EBSD orientation map of the alloy displaying a very large grain outlined in red. The inset map shows variation in crystal orientation within the same grain and highlights the presence of numerous low angle sub-boundaries.

The surface pitting was considered to arise from a combination of several causes, including: (a) cavities left by embedded lumps of oxide released during etching; (b) preferential etching of residual smeared metal revealing a grinding artefact (deep scratch); and (c) preferential etching of a particular lattice orientation (dislocations, etc., perhaps caused by a closely underlying inclusion). A thickness of 20–30 μm was observed to have been removed from the etched region which was considered to have been sufficient for the removal of all pre-existing mechanical damage arising from preparatory grinding and polishing. While the removal of mechanical damage was beneficial for subsequent EBSD analysis, the quality of the surface finish observed indicates that both the mechan-

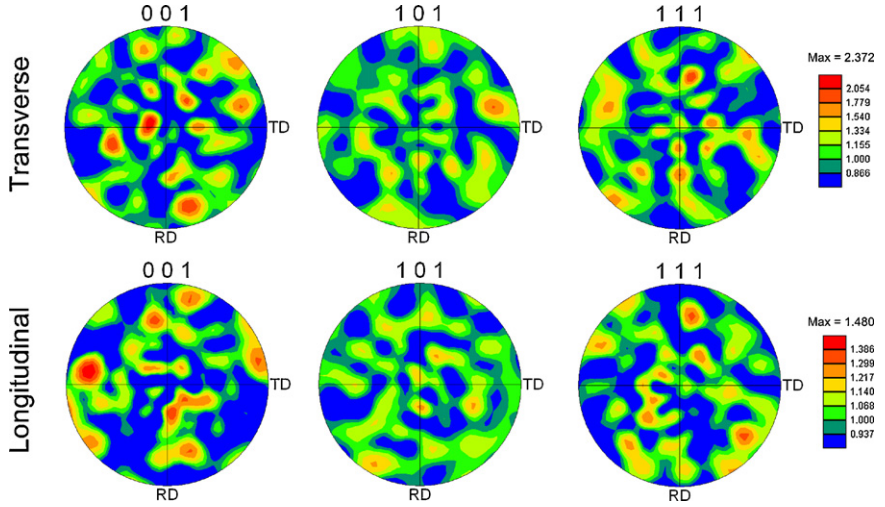

Fig. 7. Texture plots generated from grain mapping performed on the electro-polished alloy surface.

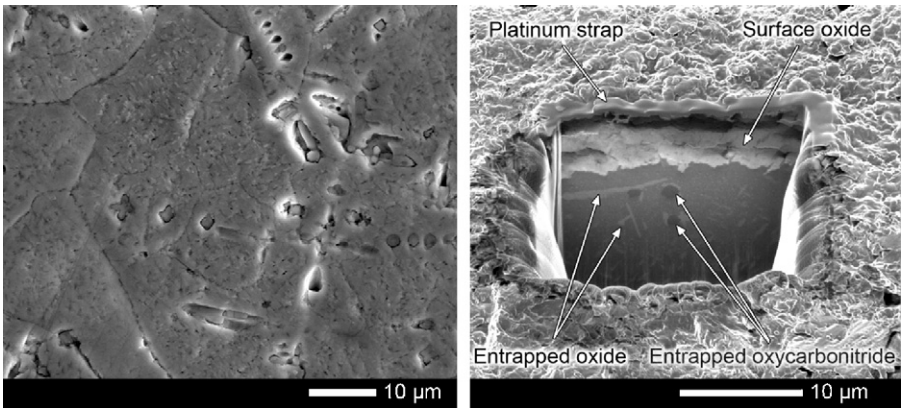

Fig. 8. Secondary electron images of the electro-polished alloy surface and of a FIB-milled section revealing a ~5 μm thick oxide layer. Both images highlight the presence of inclusions that are presumed to exist throughout the bulk metal.

ical and electro-polishing processes applied need to be further improved in order to minimise/eliminate the micro-scale surface roughness.

FIB milling was used to cut down beneath the alloy surface to a depth ~10 μm and the images of the section faces confirmed that the embedded particles observed at the alloy surfaces also existed in the bulk metal as illustrated in Fig. 8. The micro-sections produced indicate the presence of two types of entrapped particles. Most abundant were needle-like particles <0.5 μm in width ascribed as oxides on the basis that they exhibited electron channelling and *Z*-number contrasting which matched the surface oxide. Cubic particles up to 1 μm across were also observed, but with significantly less abundance, and ascribed as oxycarbonitride particles which were identified with AES (auger electron spectroscopy). This result indicates that the surface particles observed after electropolishing exist as formerly embedded particles rather than rapidly formed surface oxide, which would have been expected to exhibit greater uniformity.

Accompanying SIMS analysis, using positive ion mapping confirmed that the alloy was well mixed. Ion maps obtained for La and Ce indicated that both elements had uniform distribution across the mapped surface areas (Fig. 9). Survey mass spectra also indicated the presence of Li, Na and K as impurities, which ion mapping subsequently determined to be associated with inclusion particles (Fig. 9).

From the current investigation the primary limitation in successfully preparing alloy samples devoid of oxide for EBSD analysis was found to be in obtaining a high purity alloy. Given the melting temperatures of CeO_2 (at 2400 °C) and La_2O_3 (2315 °C) are very much higher than that of their precursor metals (798 °C and 918 °C respectively) [19,20] the oxide recorded in the SIMS data and observed by FIB imaging is considered predominantly to be present as material surviving the melting process used to form the alloy. The oxide particles are considered to arise either from that which originally coated the source metals or, as seems to be more likely given its prevalence, metal vapourised by the arc and subsequently oxidized by residual O_2 in the furnace system which was then entrained in the melt.

The presence of oxide particles embedded throughout the volume of the ingot presented a significant preparatory issue. The significantly greater hardness of particles relative to the metal (Table 1) meant that particles freed from the surface during mechanical polishing then contributed to micron-scale gouging and scratching. Considering the densities of the possible Ce and

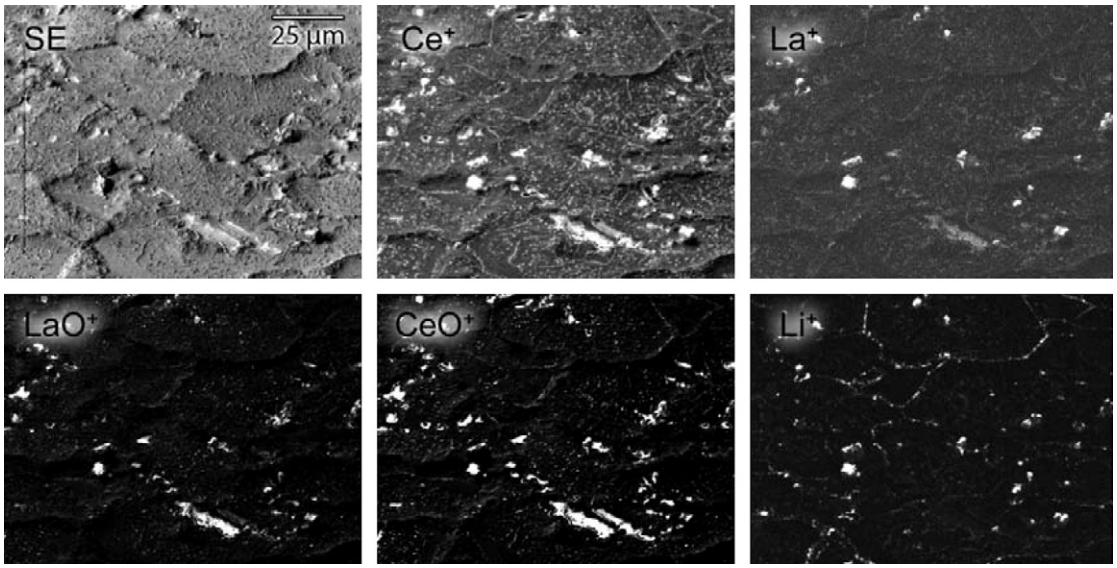

Fig. 9. A series of SIMS maps revealing the distribution of Ce and La in the metal and oxide inclusions. Li^+ was also found to exhibit similar distribution. Prior to mapping, the oxide layer on the sample surface was removed by an extended period of ion etching. The as-mapped oxide signals (LaO^+ and CeO^+) therefore indicate the presence of oxide particles extending deeper within the alloy.

Table 1
Relevant physical property-data* for Ce and La metal and their common oxides.

Metal & oxide	Crystal system	Density (g/cm^3)	Vickers hardness (GPa)	Melting point (°C)
Ce (metal)	Cubic @ 20 °C	6.77 @ 20 °C 6.55 @ 798 °C	0.27	798
La (metal)	Hexagonal	6.16 @ 20 °C 5.94 @ 918 °C	0.491	918
CeO_2	Cubic	6.86–7.30	2.98–10.3	2400
Ce_2O_3	Hexagonal	6.87	–	2177
	Cubic	6.33	–	
La_2O_3	Hexagonal	6.58	–	2250
	Cubic	5.84	–	

* Data reproduced from Gschneidner, Jr [17], Hammond [18] and references therein.

La oxides is very close to that of their respective parent metals (Table 1), it is not surprising that the arc melting process used for alloy preparation did not manage to separate out the oxide.

4. Conclusions

The current work shows that the surface of Ce–La alloy can be successfully mapped using EBSD to provide a detailed microstructural study of this material. The methods developed have demonstrated that the alloy can be successfully prepared using electro-polishing and without the need for further specialist preparation using ion beam etching. This work represents a landmark development in the preparation and analysis of cerium and similar materials, which have previously been considered too difficult to prepare in the open laboratory. Consequently this work will pave the way for further microstructual studies of Ce–La alloys and similar f-block metals that may now be undertaken by a wide range of international research groups that previously considered themselves technically excluded from such studies. Future EBSD research on cerium and cerium-lanthanum alloy will investigate the phase change behaviour of the alloy at high temperatures. Before this can be achieved, refinements in the preparation of the alloy will first be necessary to produce a material that does not contain significant amounts of oxide particles entrapped within the microstructure. It is suggested that re-melting exercises should use induction heating to avoid local vapourising hot-spots and if possible, zone-melting. Where simple gravity may not be sufficient to separate metal and oxide particles by density, surface tension of the molten metal around an oxide inclusion should be able to sweep the oxide to one end of the melt depending on how well (or not) the metal wets the embedded oxide particles.

Acknowledgements

The authors are indebted to Professor R. Harris, Drs. S. Koohpayeh and D. Ford in the Department of Metallurgy and Materials, University of Birmingham, UK, for the preparation of the Ce–La alloy.

References

[1] K.A. Gschneidner Jr., J. Alloys Compd. 180 (1992) 1–13.
[2] J-W.G. Bos, G.B.S. Penny, J.A. Rodgers, D.A. Sokolov, A.D. Huxley, J.P. Attfield, Chem. Commun. (2008) 3634–3635.
[3] W.J. Evans, J. Alloys Compd. 488 (2009) 493–510.
[4] C.M.G. dos Santos, A.J. Harte, S.J. Quinn, T. Gunnlaugsson, Coordin. Chem. Rev. 252 (2008) 2512–2527.
[5] J-C.G. Bunzli, S. Comby, A.-S. Chauvin, C.D.B. Vandevyver, J. Rare Earths 25 (2007) 257–274.
[6] Q. Luo, W.H. Wang, J. Non-Crystal. Solids 355 (2009) 759–775.
[7] Q. Wang, J.M. Pelletier, J.J. Blandin, J. Alloys Compd. 504 (2010) 357–361.
[8] D.C. Koskenmaki, K.A. Gschneidner Jr., Handbook on the Physics and Chemistry of Rare Earths, North Holland, Amsterdam, 1978, p. 1.
[9] J. Jensen, A.K. Mackintosh, Rare Earth Magnetism, Clarendon, Oxford, 1991, pp. 286–304.
[10] I.D. Hughes, M. Dane, A. Ernst, W. Hergert, M. Luders, J. Poulter, J.B. Staunton, A. Svane, Z. Szotek, W.M. Temmerman, Nature 446 (2007) 650–653.
[11] K.N.R. Taylor, M.I. Darby, Physics of Rare Earth Solids, Chapman and Hall, London, 1972.
[12] G. Strasser, G. Rosina, E. Bertel, F.P. Netzer, Surf. Sci. 152/153 (1985) 765–775.
[13] A.J. Schwartz, M. Kumar, B.L. Adams, Electron Backscatter Diffraction in Materials Science, Plenum Press, New York, 2000.
[14] C.J. Boehlert, J.D. Farr, R.K. Schulze, R.A. Pereyra, J.A. Archuleta, Phil. Mag. 83 (14) (2003) 1735–1744.
[15] Y. Jiangrong, W. Xiaolin, J. Chunli, X. Hong, L. Lei, Surf. Interface Anal. 38 (2006) 498–501.
[16] C.J. Altstetter, Metall. Mater. Trans. B 4 (12) (1973) 2723–2730.
[17] C.J. McHargue, H.L. Yakel Jr., Acta Metall. 8 (1960) 637–646.
[18] M. Zinkevich, D. Djurovic, F. Aldinger, Solid State Ionics 177 (2006) 989–1001.
[19] K.A. Gschneider Jr., Rare Earth Alloy, A Critical Review of the Alloy Systems of the Rare Earth Scandium and Yttrium Metals, D. Van Nostrand Company Inc., 1961.
[20] C.R. Hammond, Handbook of Chemistry and Physics, 81st ed., CRC Press, 2000.